ACS OMEGA

Open Access

http://pubs.acs.org/journal/acsodf

Article

Identification of a Ternary Nitride $Ti_{10}Cu_3N_4$ with a Unique Structure Type

Kyubin Hwang, Young Whan Cho, Jihyun Hong, Yunseok Kim, Jae-Hyeok Shim, Hyungsub Kim,* and Young-Su Lee*

Cite This: *ACS Omega* 2024, 9, 31035−31042

Read Online

ACCESS | Metrics & More | Article Recommendations | Supporting Information

ABSTRACT: This study presents the synthesis and detailed structural analysis of the ternary nitride $Ti_{10}Cu_3N_4$. Initially identified as Ti_3CuN within the Ti−Cu−N ternary phase diagram, its crystal structure remained unresolved and was characterized solely as belonging to the tetragonal crystal system. Through a comprehensive structural analysis, this study proposes a revised stoichiometry as $Ti_{10}Cu_3N_4$; its crystal structure represents a previously unreported structure type within the $P4_2/mnm$ space group. Its atomic arrangement was elucidated through a combination of X-ray powder diffraction profile analysis and density functional theory calculations, corroborated by neutron diffraction studies. Furthermore, the hydrogen storage properties of $Ti_{10}Cu_3N_4$ were characterized, demonstrating a hydrogen absorption capacity of approximately 0.6 wt % with desorption occurring in the temperature range of 200−550 °C.

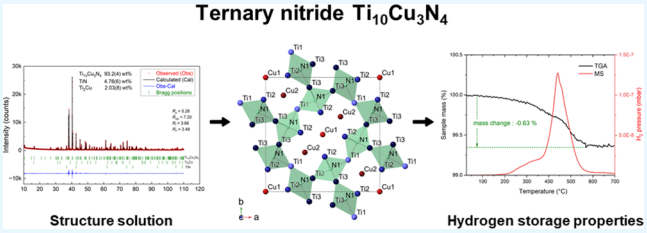

1. INTRODUCTION

Ternary nitrides have garnered significant attention in recent decades due to their diverse applications in various fields such as phosphors, battery materials, catalysts, and photovoltaics.[1] Ternary nitrides M_1-M_2-N can be classified based on the types of metal elements M_1 and M_2 (alkali, alkaline-earth, transition, precious, and post-transition metals).[2] When M_1 is an alkali or alkaline-earth metal, stable ternary nitrides are mostly normal nitrides (or N-rich nitrides) such as Ca_6GaN_5,[3] Li_3AlN_2,[4] and $SrTiN_2$.[5] However, when neither M_1 nor M_2 belongs to alkali or alkaline-earth metals, subnitrides (or N-poor nitrides) with an excess of electropositive elements are more prevalent[2] such as Ti_4Ni_2N,[6] Ti_3AlN,[7] and Mn_3CuN.[8]

Among N-poor nitrides, the extent to which N incorporation modifies the structure varies among compounds. In Ti_4Ni_2N, N occupies an octahedral interstitial position coordinated by six Ti atoms (Ti_6 sites) without changing the skeletal structure of the parent intermetallic compound Ti_2Ni. Similarly, N occupies Ti_6 octahedral sites in Ti_3AlN; however, N incorporation induces a configuration change in the metal atoms from a hexagonal close-packed (hcp) structure to a face-centered cubic (fcc) structure. Mn and Cu form a disordered fcc structure, but the N introduction stabilizes the ordered fcc metal lattice in Mn_3CuN. In cases such as $NaBa_3N$,[9] where no corresponding intermetallic compound exists, N plays a crucial role in structure stabilization.

In addition to structural effects, N incorporation can also lead to intriguing changes in physical and chemical properties, such as hydrogen sorption. For instance, Ti_2Ni forms a highly stable hydride ($Ti_2NiH_{2.9}$) at room temperature, releasing only a portion of the hydrogen to become $Ti_2NiH_{2.1}$ at temperatures as high as 460 °C.[10] Takeshita et al.[6] demonstrated that H interaction significantly weakens in Ti_4Ni_2N, enabling reversible hydrogen store and release at room temperature. The incorporation of N into the structure removes the overly stable Ti_6 sites and adjusts the stability of other interstitial sites for hydrogen absorption, making Ti_4Ni_2N a suitable material for room temperature hydrogen storage.

Inspired by these phenomena, we focused our attention on Ti−Cu−N ternary nitrides. The ternary nitride Ti_3CuN was initially identified in a phase diagram study by Durlu et al.[11] Although this compound has been reported in several other studies,[12−14] its structure remains unknown. The chemical formula Ti_3CuN indicates potential for H storage at moderate temperatures and pressures: while Ti forms a very stable hydride, combining it with the nonhydride-forming element Cu and the nonmetallic element N would reduce hydride stability, similar to the case of Ti_4Ni_2N.

In this study, we report the synthesis of Ti_3CuN and reveal through structural analysis that the correct stoichiometry of this compound is $Ti_{10}Cu_3N_4$. We discuss in detail the crystal structure of $Ti_{10}Cu_3N_4$ and explore its hydrogen storage capabilities.

Received: May 8, 2024
Revised: June 11, 2024
Accepted: June 19, 2024
Published: July 5, 2024

2. MATERIALS AND METHODS

2.1. Synthesis. The starting materials were Ti (99.5%, −325 mesh, Thermo Fisher Scientific), Cu (99.9%, −400 mesh, Thermo Fisher Scientific), and TiN (<3 μm, Sigma-Aldrich) powder. Each powder, totaling 20 g, was weighed to obtain the stoichiometric ratio of 3Ti−1Cu−1N. These powders were then placed in a 20 cm^3 vial and mixed using a mixer mill (MM-400, Retsch) operating at 20 Hz for 5 min, with this process repeated three times. The vials were reoriented after each cycle to ensure thorough mixing. Subsequently, the mixed powder was pelletized using a hydraulic press, applying a pressure of approximately 5 ton within a tungsten carbide mold (ϕ = 12 mm). Each resulting pellet had an approximate mass of 5 g. The pellets were wrapped in Ta foil, vacuum-sealed in a quartz tube, and sintered for 7 days at 850 °C. Photographs depicting the powder mixtures, as-prepared pellets, and sintered samples are shown in Figure S1.

Following the adjustment of the stoichiometry based on the initial structure solution, a sample with a revised stoichiometric ratio of 10Ti−3Cu−4N was synthesized using the same procedure. This sample was employed for both X-ray and neutron diffraction (ND) analyses.

2.2. Structure Solution. The phase fractions and crystal structures of the alloy samples were analyzed using X-ray powder diffraction (XRD) with Cu−Kα radiation (D8 ADVANCE, Bruker AXS GmbH, λ = 1.5418 Å). Approximately 0.5 g of the sample was manually crushed, sieved to 45 μm particle size, and then loaded for analysis. The diffraction studies covered a 2θ range from 10 to 110°, with a step size of 0.03° and a duration time of 10 s per step.

The peaks corresponding to the target compound were identified using the ICDD database [00-050-1475]. The crystal structure was solved using the indexing tool and Monte Carlo-type global optimization tool implemented in TOPAS software (ver. 5, Bruker AXS GmbH). Subsequently, the structure was further optimized using density functional theory (DFT) calculations.

2.3. X-ray and Neutron Diffraction and Studies. XRD data were collected using an X-ray diffractometer (Empyrean, Malvern Panalytical) in the 2θ range of 10−110°, with a step size of 0.013° and 2 s duration per step, using a monochromatic wavelength of 1.540598 Å. ND data were obtained from the High-Flux Advanced Neutron Application Reactor (HANARO) facility at the Korea Atomic Energy Research Institute (KAERI). The measurement covered a 2θ range of 0−160°, with a step size of 0.05° using a constant wavelength of 1.834467 Å. The phase fractions of each compound, along with the detailed atomic parameters for $Ti_{10}Cu_3N_4$, were determined using Rietveld refinement of both XRD and ND data. These refinements utilized a crystallographic information file generated from DFT calculations. We employed the Thompson-Cox-Hastings pseudo-Voigt function for the precise fitting of diffraction peaks. This fitting process was conducted while considering the instrumental resolution function, derived from measurements using standard reference materials: Si (SRM640f) for ND and LaB_6 (SRM660c) for XRD.

2.4. Calculation. DFT calculations were conducted using the Vienna Ab initio Simulation Package (VASP)[15] to refine the crystal structure of the compound under investigation. The Perdew−Burke−Ernzerhof generalized gradient approximation[16] was employed to evaluate the exchange-correlation energies, utilizing a projector-augmented wave (PAW) potential[17] with a plane-wave cutoff energy set at 400 eV. To enhance k-point convergence, particularly for metallic systems, the Methfessel−Paxton smearing scheme[18] with a smearing energy of 0.1 eV was employed. A 3 × 3 × 12 k-point grid was applied to a simulation cell containing two formula units (f.u.) of $Ti_{10}Cu_3N_4$, achieving a total energy convergence within 0.5 meV/atom. A similar level of precision was maintained for the convergence in the simulations of $Ti_{10}Cu_3$, Ti_2Cu, TiN, Ti (hcp Ti), and Cu (fcc Cu). For simulating the N_2 molecule, a cubic cell with dimensions of 30 × 30 × 30 Å was used. Spin-polarized calculations were performed for $Ti_{10}Cu_3N_4$ and Ti_2Cu, resulting in zero magnetic moments; thus, spin-unpolarized calculation results were used. The optimized lattice parameters and total energies obtained from the DFT calculations are listed in Table S1. Bader charge analysis was performed using a grid-based algorithm implemented in the Bader analysis program (version 1.04).[19,20]

2.5. Hydrogen Sorption Properties. The hydrogen sorption properties were evaluated using an automated Sieverts-type apparatus (GASPRO HA, Setaram) as follows: Each sample was fractured into several millimeter-sized pieces in ambient air, and approximately 1 g of the sample was promptly loaded into a stainless-steel reactor. The reactor was evacuated until the pressure reached approximately 1 Pa, after which a hydrogen pressure of 4.5 MPa was applied for 100 h at 330 °C. To evaluate the desorption properties, the sample was cooled to near room temperature to retain the absorbed hydrogen and then removed from the reactor. Approximately 40 mg of the sample was placed in an alumina crucible and subjected to analysis using a thermogravimetric analyzer (TG 209 F1 Iris, Netzsch), scanning from room temperature to 700 °C at a rate of 10 °C min^{-1}. A mass spectrometer (HPR-20 R&D, Hiden Analytical) was employed for qualitative and quantitative analyses of the desorbed gas. Additionally, XRD analysis was conducted to examine changes in the lattice parameters before and after hydrogenation/dehydrogenation.

3. RESULTS AND DISCUSSION

3.1. Structure Solution. The crystal structure was determined using the laboratory XRD data (Figure S2). The lattice parameters obtained in this study were in excellent agreement with those from a previous study[11] (Table 1),

Table 1. Experimental (EXP) and Calculated (DFT) Lattice Parameters of $Ti_{10}Cu_3N_4$[a]

lattice parameters	EXP	DFT	ref. 11
a (Å)	11.9704(3)	11.966	11.968(2)
c (Å)	3.02312(8)	3.016	3.0217(3)

[a]Lattice parameters from ref. 11 were obtained from their XRD analysis of the composition 59Ti−20Cu−21N.

confirming the analysis was performed on the same compound. The space group was initially identified as $P4_2nm$ (No. 102). Considering the reported stoichiometry of Ti_3CuN and a tetragonal system with 4-fold symmetry, it was assumed that the unit cell accommodated eight formula units of Ti_3CuN, corresponding to $Ti_{24}Cu_8N_8$. During the structure determination process, the Monte Carlo simulation suggested the occupancy at the 2a Wyckoff position (0, 0, z) in the $P4_2nm$

https://doi.org/10.1021/acsomega.4c04371
ACS Omega 2024, 9, 31035−31042

space group. Attempts to satisfy the number of metal atoms in the unit cell (24 or 8) by placing the same type of metal atom at another 2*a* site, plus one 4*b* or 4*c* site, were deemed implausible due to resulting excessively short M−M distances, constrained by half of the *c* parameter (∼1.5 Å).

Volume analysis also raises doubts about the reported stoichiometry. The volume of Ti_2Cu was reported as 46.7 Å^3/f.u.,[21] and that of Ti as 17.7 Å^3/f.u.,[22] resulting in an estimated volume of 64.4 Å^3/f.u. for Ti_3Cu. Even without considering the contribution of N to the volume, the unit cell could only accommodate 6.7 units of Ti_3CuN (432.8 Å^3[11] divided by 64.4 Å^3), suggesting a potential discrepancy in stoichiometry. The possibility of seven units of Ti_3CuN in the unit cell was ruled out due to its incompatibility with the $P4_2nm$ symmetry. Thus, the most likely scenario is six units of Ti_3CuN in the unit cell. However, $Ti_{18}Cu_6N_6$ would require the occupation of at least three types of 2*a* sites to satisfy the atomic count requirement, which is not plausible.

Subsequently, a structure solution was attempted without the constraint of the Ti_3CuN stoichiometry. Guided by chemical intuition, a Monte Carlo simulation yielded an initial solution for the atomic positions of Ti (combination of 4*c*+8*d* +8*d* Wyckoff positions), Cu (2*a*+4*c*), and N (8*d*). The resulting unit cell contained $Ti_{20}Cu_6N_8$, corresponding to the chemical formula $Ti_{10}Cu_3N_4$. Further optimization of the lattice parameters and atomic positions using DFT calculations indicated agreement with the experimental values to within 0.5% (Table 1), providing strong evidence for the accurate determination of the structure. The DFT-optimized structure was reassessed using FINDSYM,[23,24] revealing the $P4_2/mnm$ space group (No. 136) with a higher symmetry than $P4_2nm$. The atomic positions obtained from the DFT calculations are summarized in Table 2. The XRD profile, along with the profile calculated from Rietveld refinement, is presented in Figure S2.

Table 2. Optimized Atomic Positions from the DFT Calculation

site	Wyckoff position	*x*	*y*	*z*	occupancy
Ti1	4*f*	0.7765	0.7765	0	1
Ti2	8*i*	0.4802	0.6944	0	1
Ti3	8*i*	0.3825	0.9120	0	1
Cu1	2*a*	0	0	0	1
Cu2	4*g*	0.8453	0.1547	0	1
N1	8*i*	0.3024	0.0684	0	1

3.2. X-ray and Neutron Diffraction Studies. After confirming the correct formula, the ternary nitride compound was synthesized according to the revised stoichiometry of 10Ti−3Cu−4N. The crystal structure was elucidated using XRD analysis, employing a monochromatic Cu−Kα_1 wavelength (λ = 1.540598 Å), due to the complexity of the newly synthesized compounds. Figure 1a shows the results of the Rietveld refinement of the XRD patterns, and the atomic positions are summarized in Table S2. The synthesized sample predominantly comprised $Ti_{10}Cu_3N_4$, with minor amounts of TiN and Ti_2Cu detected, as shown in Figure 1a. The refined lattice parameters of $Ti_{10}Cu_3N_4$ (Table S2) were almost identical to those obtained from the 3Ti−1Cu−1N sample and a previous study (Table 1). The atomic positions listed in Table S2 closely corresponded with the calculated values, further confirming the crystal structure solution. In the 10Ti−3Cu−4N sample, while a single phase was observed, minor amounts of Ti_2Cu and TiN were also present, similar to observations in the 3Ti−1Cu−1N sample where traces of Ti_2Cu and TiCu were detected (Figure S2). Although the general trend holds—an increase in N content and a decrease in Cu content in the 10Ti−3Cu−4N sample compared to the 3Ti−1Cu−1N sample resulting in TiN secondary phase formation in place of TiCu—there remains the possibility of partial occupation of the N1 site or antisite disorder between the Ti and Cu sites. The presence of secondary phases suggests a deviation from ideal stoichiometry. In the reported results (Table S2), such disorders were not considered, with the site occupancy fixed at 1 for all sites.

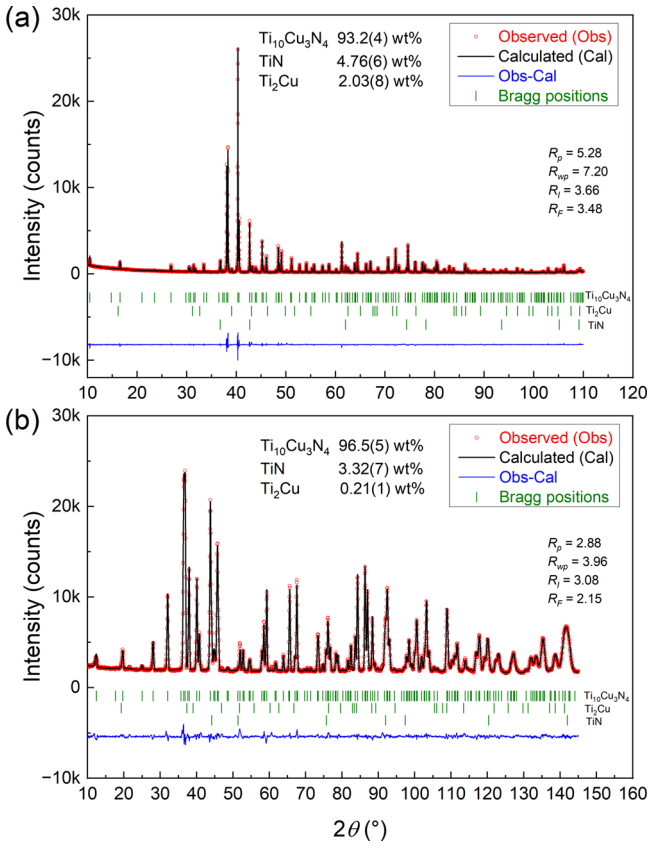

Figure 1. Obtained (a) XRD and (b) ND profiles, along with the corresponding calculated profiles from Rietveld refinement. Phase fractions and *R* values (in %) are shown in each panel.

We conducted an ND analysis, as presented in Figure 1b, with a fixed occupancy of 1 for all atomic sites. Rietveld refinement of the ND pattern yielded results closely matching those from the XRD and DFT analyses, including the lattice parameters and atomic positions (Table 3). To further investigate the occupancy of the light element N and its potential disorder within the crystalline lattice, we removed the occupancy constraint for N in the Rietveld refinement. The refined occupancy of N1 was found to be 0.994(2), which is close to 1. In addition, exploration of site exchange across all six pairs (involving three Ti and two Cu sites) indicated negligible refined exchange. Therefore, we conclude that the composition deviates minimally, if at all, from ideal stoichiometry. The presence of secondary phases can be attributed to incomplete reactions during the formation of ternary compounds.

https://doi.org/10.1021/acsomega.4c04371
ACS Omega 2024, 9, 31035−31042

Table 3. Fractional Coordinates and B_{iso} Values of the Symmetrically Distinct Atomic Sites in $Ti_{10}Cu_3N_4$ from the Rietveld Refinement of the ND Profile[a]

site	Wyckoff position	x	y	z	B_{iso}	occupancy
Ti1	4*f*	0.7774(2)	0.7774(2)	0	0.55(6)	1
Ti2	8*i*	0.4821(2)	0.6943(2)	0	0.40(4)	1
Ti3	8*i*	0.3827(2)	0.9128(2)	0	0.52(5)	1
Cu1	2*a*	0	0	0	0.78(4)	1
Cu2	4*g*	0.84386(9)	0.15614(9)	0	0.65(3)	1
N1	8*i*	0.30178(7)	0.06781(8)	0	0.65(2)	1

[a]Lattice parameters are a = 11.97178(9) Å and c = 3.02285(2) Å, and the unit cell volume is 433.246(6) Å^3.

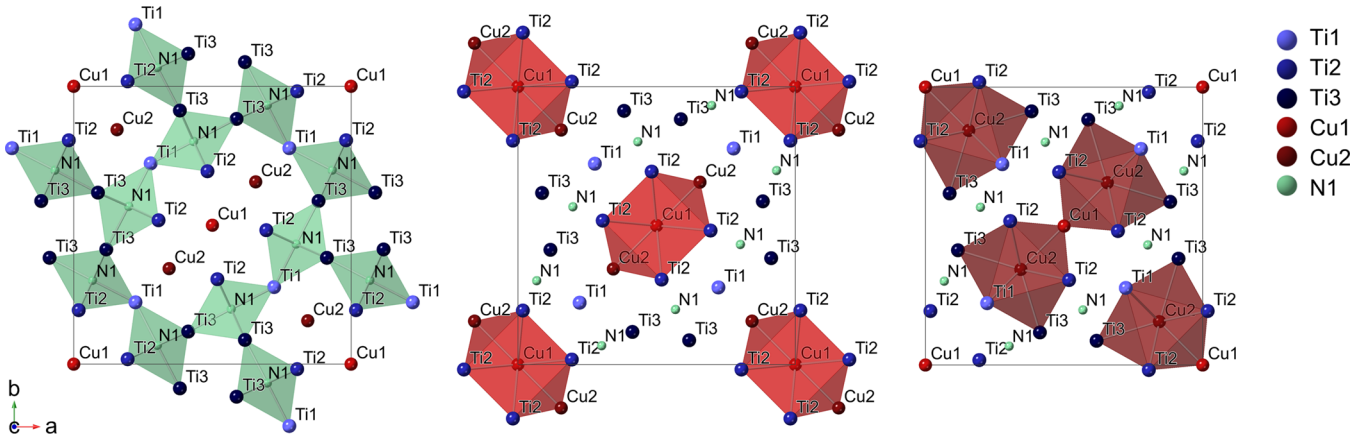

Figure 2. Crystal structure of $Ti_{10}Cu_3N_4$. N1, Cu1, and Cu2-centered polyhedra are shown in the left, center, and right panels, respectively.

3.3. Crystal Structure of $Ti_{10}Cu_3N_4$. Crystal structures obtained from the ND study are shown in Figure 2. N atoms (labeled N1) occupy octahedral sites formed by six Ti atoms: namely one Ti1, two Ti2, and three Ti3, as summarized in Table 4. Each octahedron is connected to seven other octahedra through edge sharing (Ti2−Ti3 edge) and corner sharing. Ti1 and Ti2 each have two nearest neighboring N atoms, whereas Ti3 has three, as listed in Table 4. Consequently, Ti3 primarily contributes to the complex network of the octahedra. Neglecting the contribution of Ti2, given that the Ti2−Ti3 edge is shared by Ti3, one Ti1 atom is linked to a nearby octahedron, and each of the three Ti3 atoms is connected to two other independent octahedra, resulting in a total of seven connected octahedra. Conversely, Ti2 primarily contributes to the Ti−Cu bonding network. As illustrated in Figure 2, the remaining bonding network comprises interwoven polyhedra centered at Cu1 and Cu2 stacked along the *c*-axis, with Ti2 atoms predominantly constituting this network (Table 4). This arrangement appears to represent a new type of structure. Notably, the structure-type definition list in the ICSD database[25,26] lacks entries corresponding to the space group $P4_2/mnm$ with a Pearson symbol *tP*34 and a Wyckoff sequence of (*i*3 *g f a*).

Table 4. Nearest Neighbors and Interatomic Distances for Each Site[a]

site pair		no.	distance (Å)	site pair		no.	distance (Å)
Ti1	N1	2	2.082(3)	Cu1	Cu2	2	2.644(1)
(12)	Cu2	2	2.549(3)	(10)	Ti2	8	2.782(2)
	Ti2	4	2.900(3)	Cu2	Ti1	2	2.549(3)
	Ti3	4	3.009(3)	(9)	Ti2	4	2.614(3)
Ti2	N1	2	2.073(2)		Cu1	1	2.644(1)
(12)	Cu2	2	2.614(3)		Ti3	2	2.835(3)
	Cu1	2	2.782(2)	N1	Ti2	2	2.073(2)
	Ti3	1	2.873(4)	(6)	Ti1	1	2.082(3)
	Ti1	2	2.900(3)		Ti3	1	2.094(3)
	Ti2	1	2.986(5)		Ti3	2	2.097(2)
	Ti3	2	2.993(3)				
Ti3	N1	1	2.094(3)				
(12)	N1	2	2.097(2)				
	Cu2	1	2.835(3)				
	Ti2	1	2.873(4)				
	Ti3	4	2.901(3)				
	Ti2	2	2.993(3)				
	Ti1	2	3.009(3)				

[a]Number in the parentheses right below the site symbol represents the total number of nearest neighbors. Numbers in the 3rd and 7th columns (No.) are the nearest atom count of the same type.

Although not identical, we found that this structure is a variant of previously known structures $Ca_{11}N_8$,[27] $Ca_{11}N_6(CN_2)_2$,[28] and $Na_{1.7}Ti_6O_{11}$;[29] they all belong to the space group $P4_2/mnm$, and their structures are shown in Figure S3. Compared to the $Ti_{10}Cu_3N_4$ structure, a common feature of these three structures is the presence of infinite chains of NCa_6 or TiO_6 octahedra (colored in orange in Figure S3) stacked along the *c*-axis, forming a framework of strong metal-nonmetal bonding. In $Ti_{10}Cu_3N_4$, the center of the octahedron is absent, and these metal-nonmetal bonds are replaced by intermetallic bonds, illustrated as Cu1-centered polyhedra in Figure 2. Second, N3 (in $Ca_{11}N_8$), CN_2^{2-} (in $Ca_{11}N_6(CN_2)_2$) and Na1 (in $Na_{1.7}Ti_6O_{11}$) are located in one-dimension channels formed by a framework composed of polyhedra[28] (as shown in Figure S3). These atoms or anionic ligands are rather loosely bound to the atoms forming the framework; for instance, Ca1−N3 distances (in $Ca_{11}N_8$) are longer than other

https://doi.org/10.1021/acsomega.4c04371
ACS Omega 2024, 9, 31035−31042

Ca−N distances, and the Na1 position is partially filled in $Na_{1.7}Ti_6O_{11}$. This structural flexibility is evidenced by the replacement of N3 (in $Ca_{11}N_8$) with CN_2^{2-} (in $Ca_{11}N_6(CN_2)_2$). In contrast, Cu2 atoms form tight bonds with nearby Ti atoms, as shown by the bond distances in Table 4. Lastly, N1 in $Ca_{11}N_8$ (or N2 in $Ca_{11}N_6(CN_2)_2$) forms an NCa_5 rectangular base pyramid[27] (colored in green in Figure S3), which differs from an NTi_6 octahedron in $Ti_{10}Cu_3N_4$. On the other hand, Ti1 in $Na_{1.7}Ti_6O_{11}$ forms a TiO_6 octahedron similar to the NTi_6 octahedron in $Ti_{10}Cu_3N_4$. However, its Ti1−O3 distance (2.242 Å) is noticeably longer than the Ti1−O2 distance (1.947 Å), resulting in a distorted octahedron.[29] In contrast, the corresponding bond distances (2.082 and 2.094 Å) in $Ti_{10}Cu_3N_4$ differ by only 0.012 Å, forming a much more regular NTi_6 octahedron.

3.4. Stability and Electronic Structure. The stability assessment of $Ti_{10}Cu_3N_4$ was conducted using DFT total energy calculations. The predictions indicated a negative formation energy (eq 1) when synthesizing $Ti_{10}Cu_3N_4$ from the starting materials, Ti (hcp Ti), Cu (fcc Cu), and TiN, consistent with experimental observations. Similarly, the formation energy of $Ti_{10}Cu_3N_4$ from the two major secondary phases, Ti_2Cu and TiN, was negative (eq 2), confirming the stability of $Ti_{10}Cu_3N_4$.

$$6Ti + 3Cu + 4TiN \rightarrow Ti_{10}Cu_3N_4 \quad \Delta E = -3.14 \text{ eV } (-0.18 \text{ eV/atom}) \tag{1}$$

$$3Ti_2Cu + 4TiN \rightarrow Ti_{10}Cu_3N_4 \quad \Delta E = -2.06 \text{ eV } (-0.12 \text{ eV/atom}) \tag{2}$$

The exceptional stability of the binary nitride TiN (eq 3) highlights $Ti_{10}Cu_3N_4$ as a rare example of a highly stable Ti-M_2-N ternary nitride, with M_2 representing a late transition metal. The formation energy of $Ti_{10}Cu_3N_4$ from Ti, Cu, and N_2 was −1.00 eV/atom (eq 4).

$$Ti + 1/2N_2 \rightarrow TiN \quad \Delta E = -3.47 \text{ eV } (-1.73 \text{ eV/atom}) \tag{3}$$

$$10Ti + 3Cu + 2N_2 \rightarrow Ti_{10}Cu_3N_4 \quad \Delta E = -17.0 \text{ eV } (-1.00 \text{ eV/atom}) \tag{4}$$

Simulations on a hypothetical compound, $Ti_{10}Cu_3$, were conducted to determine the primary stabilizing factor of $Ti_{10}Cu_3N_4$ by decomposing the overall stability into metal−metal and metal−nonmetal interactions. We italicize $Ti_{10}Cu_3$ to indicate that this is a hypothetical compound. Eliminating the N atoms in $Ti_{10}Cu_3N_4$, structural optimization resulted in slightly contracted lattice parameters (Table S1). The formation energy of the hypothetical compound $Ti_{10}Cu_3$ from Ti and Cu exhibited only marginal negativity (eq 5), in contrast with the considerably negative formation energy of $Ti_{10}Cu_3N_4$ (eq 4). Consistent with the Ti−Cu phase diagram, which illustrates the absence of intermetallic compounds between Ti and Ti_2Cu,[30] the formation energy of $Ti_{10}Cu_3$ from Ti and Ti_2Cu was positive (eq 6). Consequently, we posit N plays an important role in enhancing the stability of the structure. The formation energy of $Ti_{10}Cu_3N_4$ from $Ti_{10}Cu_3$ and N_2 (eq 7) predominantly contributes to the overall energy in eq 4.

$$10Ti + 3Cu \rightarrow Ti_{10}Cu_3 \quad \Delta E = -0.31 \text{ eV } (-0.02 \text{ eV/atom}) \tag{5}$$

$$4Ti + 3Ti_2Cu \rightarrow Ti_{10}Cu_3 \quad \Delta E = 0.77 \text{ eV } (0.06 \text{ eV/atom}) \tag{6}$$

$$Ti_{10}Cu_3 + 2N_2 \rightarrow Ti_{10}Cu_3N_4 \quad \Delta E = -16.7 \text{ eV } (-0.98 \text{ eV/atom}) \tag{7}$$

Robust bonding between the Ti and N atoms is evident in the electronic density of states of $Ti_{10}Cu_3N_4$ depicted in Figure 3. A substantial overlap occurs between the partial density of states of the Ti and N atoms below −4 eV, whereas the Cu−N overlap remains minimal, as expected from the atomic arrangement (Figure 2 and Table 4). A narrow *d*-band of Cu is situated between −4 and −2 eV, and Ti dominates the states around the Fermi energy (E_F), indicating the metallic characteristics of the compound, which is consistent with the black color of the synthesized compound (Figure S1).

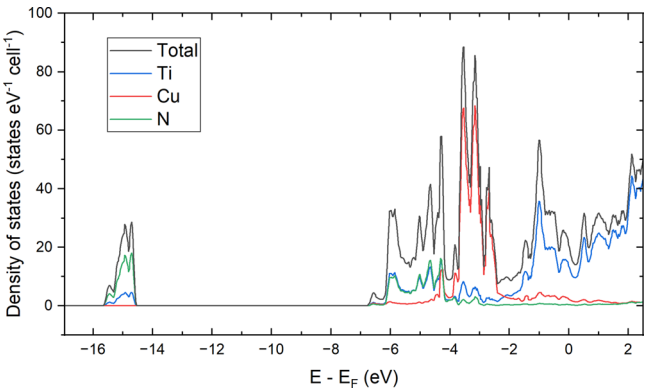

Figure 3. Electronic structure of $Ti_{10}Cu_3N_4$. Total density of states (black) and partial density of states projected to Ti (blue), Cu (red), and N (green) atoms are coplotted.

Further examination of the bonding involved analyzing the charge distribution at each site via Bader charge analysis of $Ti_{10}Cu_3N_4$ and $Ti_{10}Cu_3$. The results are summarized in Table 5. As expected, Ti atoms exhibited positive net atomic charges, whereas Cu and N atoms displayed negative charges owing to their higher electronegativity. Among the distinct Ti sites, Ti2, which has the largest number of N and Cu neighbors (Table 4), exhibited the highest net charge, followed by Ti3 with three N neighbors, albeit with negligible differences among the Ti sites. Similarly, Cu2, which forms shorter bonds with the Ti atoms (Table 4), withdraws more electrons from Ti. Upon N incorporation, the positive charge on the Ti sites in $Ti_{10}Cu_3N_4$

Table 5. Net Atomic Charges on Ti, Cu, and N Sites within the $Ti_{10}Cu_3N_4$ and Hypothetical $Ti_{10}Cu_3$ Structure, Obtained from the Bader Charge Analysis

site	$Ti_{10}Cu_3N_4$	$Ti_{10}Cu_3$
Ti1	1.07	0.45
Ti2	1.11	0.42
Ti3	1.09	0.17
Cu1	−0.95	−0.79
Cu2	−1.26	−1.23
N1	−1.87	

https://doi.org/10.1021/acsomega.4c04371
ACS Omega 2024, 9, 31035−31042

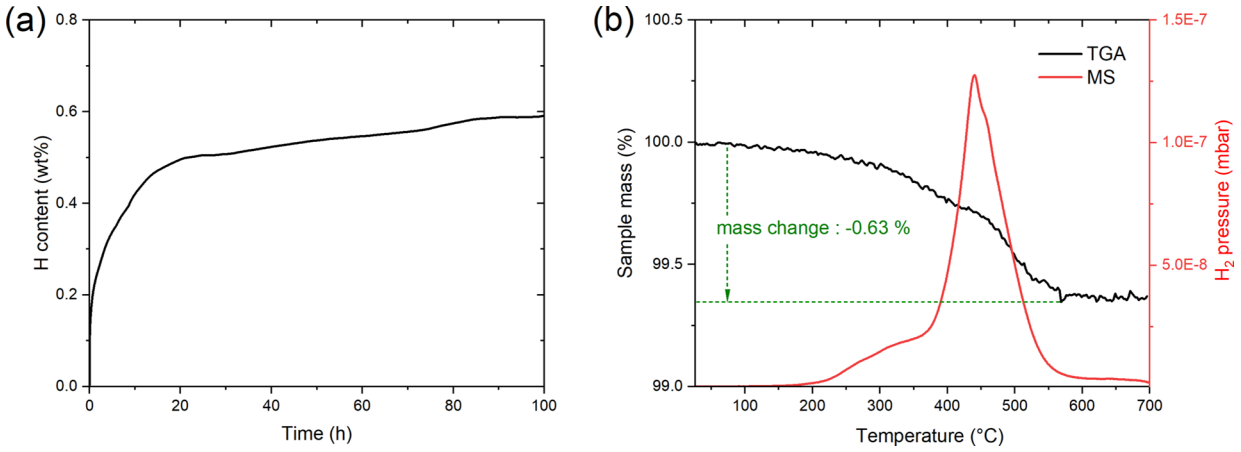

Figure 4. (a) Hydrogen absorption data of $Ti_{10}Cu_3N_4$ at 330 °C under 4.5 MPa of H_2 pressure. (b) Thermogravimetric analysis (TGA, in black) and mass spectrometry result (MS, in red) of hydrogenated $Ti_{10}Cu_3N_4$.

notably increases, particularly in Ti3, which has three nearest N neighbors. The increase in positive charges on the Ti sites induced by N strengthens the Ti−Cu bonding through the generation of more polar bonds. Additionally, the charge on the Cu sites became slightly more negative after N incorporation. Enhanced Ti−Cu bonding is corroborated by DFT calculations, demonstrating reduced Ti−Cu bond distances in $Ti_{10}Cu_3N_4$ compared to $Ti_{10}Cu_3$ (Table S3), with Cu2−Ti3 displaying the most significant reduction, consistent with Ti3's pronounced charge increase. These findings collectively underscore the crucial role of N in enhancing the stability of $Ti_{10}Cu_3N_4$.

3.5. Hydrogen Storage Characteristics. The initial hydrogen absorption (or activation) curve of $Ti_{10}Cu_3N_4$ compound at 330 °C under a hydrogen pressure of 4.5 MPa is shown in Figure 4a. Attempts to activate the sample at room temperature were unsuccessful, necessitating activation at 330 °C. Initially, the sample readily absorbed hydrogen up to approximately 0.2 wt %; however, thereafter, the absorption kinetics slowed considerably, with approximately 0.6 wt % of hydrogen being absorbed over a 100 h period. Notably, this hydrogen absorption did not induce structural changes; instead, the lattice parameters increased with hydrogenation (Table S4). The cell volume of the $Ti_{10}Cu_3N_4$ phase increased by approximately 2.2% after 100 h of hydrogenation (from 433.4 to 442.9 $Å^3$). Once hydrogenated, the $Ti_{10}Cu_3N_4$ compound was capable of absorbing hydrogen even at room temperature; however, it did not desorb hydrogen unless exposed to high temperatures.

Thermogravimetric analysis combined with mass spectrometry (TGA-MS) was performed to assess the hydrogen desorption properties of the hydrogenated $Ti_{10}Cu_3N_4$. The temperature was increased at a scanning rate of 10 °C min^{-1}. The results are presented in Figure 4b. According to the MS data, hydrogen was desorbed over a wide range of temperatures, starting at approximately 200 °C, peaking at approximately 450 °C, and completing below 600 °C. Owing to the complex crystal structure of $Ti_{10}Cu_3N_4$, various sites with different binding energies exist within the $Ti_{10}Cu_3N_4$ structure for H atoms to occupy. Consequently, H atoms occupying unstable positions were released at relatively low temperatures, whereas H atoms in stable positions were desorbed at higher temperatures. The cell volume after TGA returned to that of the as-sintered $Ti_{10}Cu_3N_4$ before hydrogenation (Table S4), indicating the loss of H from the structure.

Our initial motivation for studying the Ti−Cu−N compound was to design a hydrogen storage material that is less stable than pure Ti. Therefore, we compared the stability of the hydrogenated $Ti_{10}Cu_3N_4$ with that of TiH_2. Studies investigating the dehydrogenation of TiH_2 using TGA reported initiation of dehydrogenation at approximately 450 °C, peaking near 550 °C, and completing around 800 °C.[31,32] The TGA-MS results presented in Figure 4b demonstrate that $Ti_{10}Cu_3N_4$ formed less stable hydrides than Ti. However, its relatively low hydrogen storage capacity limits its use as a hydrogen storage material. We could not ascertain whether this capacity represented the maximum hydrogen storage capacity of the compound. Given the slow kinetics observed, the absorption process was halted at 100 h. Nevertheless, optimization of the temperature/pressure conditions and the adoption of different synthesis conditions may enable this compound to absorb larger amounts of hydrogen, necessitating further investigation.

4. CONCLUSIONS

In summary, this study provides a comprehensive investigation of the crystal structure, stability, and hydrogen storage properties of Ti−Cu−N ternary nitrides. Through a combination of crystal structure determination from XRD data and DFT calculations, we elucidated the stoichiometry of $Ti_{10}Cu_3N_4$, correcting its prior misidentification as Ti_3CuN. Rietveld refinement performed on the ND profile further confirmed that the composition deviated minimally from the ideal stoichiometry of $Ti_{10}Cu_3N_4$. Notably, the crystal structure of $Ti_{10}Cu_3N_4$ represents a novel addition to the inorganic crystal structure repository. Our analysis of the thermodynamic stability highlights the importance of metal−nonmetal bonding in stabilizing this ternary nitride. $Ti_{10}Cu_3N_4$ exhibits a hydrogen absorption capacity of approximately 0.6 wt % and demonstrates hydrogen desorption at lower temperatures than TiH_2. This observation aligns with the concept of utilizing Cu and N to design less stable hydrides.

■ ASSOCIATED CONTENT

Supporting Information

The Supporting Information is available free of charge at https://pubs.acs.org/doi/10.1021/acsomega.4c04371.

https://doi.org/10.1021/acsomega.4c04371
ACS Omega 2024, 9, 31035−31042

DFT-calculated lattice parameters and total energies of the compounds investigated; fractional coordinates and B_{iso} values of the symmetrically distinct atomic sites in $Ti_{10}Cu_3N_4$ from the Rietveld refinement of the XRD profile; nearest neighbors and interatomic distances for Cu sites from the DFT-optimized structure of $Ti_{10}Cu_3N_4$ and $Ti_{10}Cu_{3;}$ lattice parameters and volume changes of as-sintered, hydrogenated, and dehydrogenated $Ti_{10}Cu_3N_4$; sample preparation; obtained laboratory XRD profile and the calculated profile from Rietveld refinement for the 3Ti−1Cu−1N sample; and crystal structure of (a) $Ca_{11}N_8$, (b) $Ca_{11}N_6(CN_2)_2$, and (c) $Na_{1.7}Ti_6O_{11}$ (PDF)

AUTHOR INFORMATION

Corresponding Authors

Hyungsub Kim − *Neutron Science Division, Korea Atomic Energy Research Institute (KAERI), Daejeon 34057, Republic of Korea*; Email: hyungsubkim@kaeri.re.kr

Young-Su Lee − *Energy Materials Research Center, Korea Institute of Science and Technology (KIST), Seoul 02792, Republic of Korea*; orcid.org/0000-0002-3160-6633; Email: lee0su@kist.re.kr

Authors

Kyubin Hwang − *Energy Materials Research Center, Korea Institute of Science and Technology (KIST), Seoul 02792, Republic of Korea; School of Advanced Materials Science and Engineering, Sungkyunkwan University (SKKU), Suwon 16419, Republic of Korea*; orcid.org/0009-0007-7576-0249

Young Whan Cho − *Energy Materials Research Center, Korea Institute of Science and Technology (KIST), Seoul 02792, Republic of Korea*

Jihyun Hong − *Energy Materials Research Center, Korea Institute of Science and Technology (KIST), Seoul 02792, Republic of Korea*; orcid.org/0000-0001-7210-2901

Yunseok Kim − *Energy Materials Research Center, Korea Institute of Science and Technology (KIST), Seoul 02792, Republic of Korea; School of Advanced Materials Science and Engineering and KIST-SKKU Carbon-Neutral Research Center, Sungkyunkwan University (SKKU), Suwon 16419, Republic of Korea*; orcid.org/0000-0003-1794-1248

Jae-Hyeok Shim − *Energy Materials Research Center, Korea Institute of Science and Technology (KIST), Seoul 02792, Republic of Korea; School of Advanced Materials Science and Engineering and KIST-SKKU Carbon-Neutral Research Center, Sungkyunkwan University (SKKU), Suwon 16419, Republic of Korea*

Complete contact information is available at: https://pubs.acs.org/10.1021/acsomega.4c04371

Notes

The authors declare no competing financial interest.

ACKNOWLEDGMENTS

This study was financially supported by the Korea Institute of Science and Technology (grant nos. 2E33262 and 2E32591-23-085) and the "Technology Development Program to Solve Climate Change" of the National Research Foundation, funded by the Ministry of Science and ICT (NRF-2020M1A2A2080881). This study was also supported by the Commercialization Promotion Agency for R&D Outcomes (COMPA) grant funded by the Korean Government (Ministry of Science and ICT) (RS-2023-00304772).

REFERENCES

(1) Greenaway, A. L.; Melamed, C. L.; Tellekamp, M. B.; Woods-Robinson, R.; Toberer, E. S.; Neilson, J. R.; Tamboli, A. C. Ternary Nitride Materials: Fundamentals and Emerging Device Applications. *Annu. Rev. Mater. Res.* **2021**, *51*, 591−618.

(2) Sun, W.; Bartel, C. J.; Arca, E.; Bauers, S. R.; Matthews, B.; Orvañanos, B.; Chen, B.-R.; Toney, M. F.; Schelhas, L. T.; Tumas, W.; et al. A Map of the Inorganic Ternary Metal Nitrides. *Nat. Mater.* **2019**, *18*, 732−739.

(3) Cordier, G.; Kniep, R.; Höhn, P.; Rabenau, A. Ca_6GaN_5 und Ca_6FeN_5. Verbindungen mit $[CO_3]^{2-}$-Isosteren Anionen $[GaN_3]^{C-}$ und $[FeN_3]^{6-}$. *Z. Anorg. Allg. Chem.* **1990**, *591*, 58−66.

(4) Yamane, H.; Kikkawa, S.; Koizumi, M. Lithium Aluminum Nitride, Li_3AlN_2 as a Lithium Solid Electrolyte. *Solid State Ionics* **1985**, *15*, 51−54.

(5) Gregory, D. H.; Barker, M. G.; Edwards, P. P.; Siddons, D. J. Synthesis and Structure of the New Ternary Nitride $SrTiN_2$. *Inorg. Chem.* **1998**, *37*, 3775−3778.

(6) Takeshita, H. T.; Tanaka, H.; Kuriyama, N.; Sakai, T.; Uehara, I.; Haruta, M. Hydrogenation Characteristics of Ternary Alloys Containing Ti_4Ni_2X (X = O, N, C). *J. Alloys Compd.* **2000**, *311*, 188−193.

(7) Schuster, J. C.; Bauer, J. The Ternary System Titanium-Aluminum-Nitrogen. *J. Solid State Chem.* **1984**, *53*, 260−265.

(8) Barberon, M.; Madar, R.; Fruchart, M. E.; Lorthioir, G.; Fruchart, R. Les Deformations Quadratiques T1 Et T4 Dans Les Carbures Et Nitrures Perowskites Du Manganese. *Mater. Res. Bull.* **1970**, *5*, 1−7.

(9) Rauch, P. E.; Simon, A. The New Subnitride $NaBa_3N$; an Extension of Alkali Metal Suboxide Chemistry. *Angew. Chem., Int. Ed.* **1992**, *31*, 1519−1521.

(10) Mintz, M. H.; Hadari, Z.; Dariel, M. P. Hydrogenation Characteristics of Ti_2NiO_x Compounds ($0 \leqslant X < 0.5$). *J. Less-Common Met.* **1979**, *63*, 181−191.

(11) Durlu, N.; Gruber, U.; Pietzka, M. A.; Schmidt, H.; Schuster, J. C. Phases and Phase Equilibria in the Quaternary System Ti−Cu−Al−N at 850 °C. *Z. Metallkd.* **1997**, *88*, 390−400.

(12) Raghavan, V. Al−Cu−N−Ti (Aluminum-Copper-Nitrogen-Titanium). *J. Phase Equilib. Diffus.* **2006**, *27*, 171−172.

(13) Li, J.; Chen, C.; He, Q. Influence of Cu on Microstructure and Wear Resistance of TiC/TiB/TiN Reinforced Composite Coating Fabricated by Laser Cladding. *Mater. Chem. Phys.* **2012**, *133*, 741−745.

(14) Mukhopadhyay, A. K.; Roy, A.; Bhattacharjee, G.; Das, S. C.; Majumdar, A.; Wulff, H.; Hippler, R. Surface Stoichiometry and Depth Profile of Ti_x-Cu_yN_z Thin Films Deposited by Magnetron Sputtering. *Materials* **2021**, *14*, 3191.

(15) Kresse, G.; Furthmüller, J. Efficient Iterative Schemes for Ab Initio Total-Energy Calculations Using a Plane-Wave Basis Set. *Phys. Rev. B* **1996**, *54*, 11169−11186.

(16) Perdew, J. P.; Burke, K.; Ernzerhof, M. Generalized Gradient Approximation Made Simple. *Phys. Rev. Lett.* **1996**, *77*, 3865−3868.

(17) Blöchl, P. E. Projector Augmented-Wave Method. *Phys. Rev. B* **1994**, *50*, 17953−17979.

(18) Methfessel, M.; Paxton, A. T. High-Precision Sampling for Brillouin-Zone Integration in Metals. *Phys. Rev. B* **1989**, *40*, 3616−3621.

(19) Sanville, E.; Kenny, S. D.; Smith, R.; Henkelman, G. Improved Grid-Based Algorithm for Bader Charge Allocation. *J. Comput. Chem.* **2007**, *28*, 899−908.

(20) Tang, W.; Sanville, E.; Henkelman, G. A Grid-Based Bader Analysis Algorithm without Lattice Bias. *J. Phys.: Condens. Matter* **2009**, *21*, No. 084204.

(21) Mueller, M. H.; Knott, H. W. *The Crystal Structures of Ti_2Cu, Ti_2Ni, Ti_4Ni_2O, and Ti_4Cu_2O*; Argonne National Laboratory, contract no. W-31-109-eng-38: 1962.
(22) Sabeena, M.; Murugesan, S.; Anees, P.; Mohandas, E.; Vijayalakshmi, M. Crystal Structure and Bonding Characteristics of Transformation Products of bcc β in Ti-Mo Alloys. *J. Alloys Compd.* **2017**, *705*, 769−781.
(23) Stokes, H. T.; Hatch, D. M.; Campbell, B. J. *Findsym, Isotropy Software Suite*.
(24) Stokes, H. T.; Hatch, D. M. Findsym: Program for Identifying the Space-Group Symmetry of a Crystal. *J. Appl. Crystallogr.* **2005**, *38*, 237−238.
(25) ICSD Version 5.1.0 (ICSD Release 2023.2). https://icsd.fiz-karlsruhe.de/.
(26) Zagorac, D.; Müller, H.; Ruehl, S.; Zagorac, J.; Rehme, S. Recent Developments in the Inorganic Crystal Structure Database: Theoretical Crystal Structure Data and Related Features. *J. Appl. Crystallogr.* **2019**, *52*, 918−925.
(27) Laurent, Y.; Lang, J.; Le Bihan, M.-T. Structure D'un Nouveau Nitrure De Calcium: $Ca_{11}N_8$. *Acta Crystallogr., Sect. B* **1969**, *25*, 199−203.
(28) Bowman, A.; Smith, R. I.; Gregory, D. H. 3D Nitride Frameworks with Variable Channel Sizes; Synthesis and Powder Neutron Diffraction Study of the Nitride Carbodiimdes, $Ca_4N_2(CN_2)$ and $Ca_{11}N_6(CN_2)_2$. *Top. Catal.* **2009**, *52*, 1598−1603.
(29) Akimoto, J.; Takei, H. $Na_{1.7}Ti_6O_{11}$: A New Mixed-Valence Nonstoichiometric Sodium Titanate with a Tunnel Structure. *J. Solid State Chem.* **1990**, *85*, 8−14.
(30) Murray, J. L. The Cu−Ti (Copper-Titanium) System. *Bull. Alloy Phase Diagr.* **1983**, *4*, 81−95.
(31) Bhosle, V.; Baburaj, E. G.; Miranova, M.; Salama, K. Dehydrogenation of TiH_2. *Mater. Sci. Eng., A* **2003**, *356*, 190−199.
(32) Liu, H.; He, P.; Feng, J. C.; Cao, J. Kinetic Study on Nonisothermal Dehydrogenation of TiH_2 Powders. *Int. J. Hydrogen Energy* **2009**, *34*, 3018−3025.

https://doi.org/10.1021/acsomega.4c04371
ACS Omega 2024, 9, 31035−31042